# 19 Slider Crank

## 19.1 General Information

This problem was contributed by Bernd Simeon, March 1998. The slider crank shows some typical properties of simulation problems in *flexible multibody systems*, i.e., constrained mechanical systems which include both rigid and elastic bodies. It is also an example of a *stiff mechanical system* since it features large stiffness terms in the right hand side. Accordingly, there are some fast variables with high frequency oscillations.

This problem is originally described by a second order system of differential-algebraic equations (DAEs), but transformed to first order and semi-explicit system of dimension 24. The index of the problem is originally 3, but an index 1 and index 2 formulation are supplied as well. By default, the subroutines provide the index 2 formulation.

Comments to `simeon@ma.tum.de`.

The software part of the problem is in the file crank.f available at [MM08].

## 19.2 Mathematical description of the problem

The original problem has the form

$$\begin{aligned} \boldsymbol{M}(p,q)\begin{pmatrix} \ddot{p} \\ \ddot{q} \end{pmatrix} &= \boldsymbol{f}(p,\dot{p},q,\dot{q}) - \boldsymbol{G}(p,q)^{\mathrm{T}}\lambda, \\ 0 &= \boldsymbol{g}(p,q) + \boldsymbol{r}(t), \end{aligned} \tag{II.19.1}$$

where $0 \le t \le 0.1$, $p \in \mathbb{R}^3$, $q \in \mathbb{R}^4$, $\lambda \in \mathbb{R}^3$, $\boldsymbol{M} : \mathbb{R}^7 \to \mathbb{R}^7 \times \mathbb{R}^7$, $\boldsymbol{f} : \mathbb{R}^{14} \to \mathbb{R}^7$, $\boldsymbol{g} : \mathbb{R}^7 \to \mathbb{R}^3$, $\boldsymbol{r} : \mathbb{R} \to \mathbb{R}^3$, and $\boldsymbol{G} = \partial \boldsymbol{g}/\partial(p,q)$. The matrix $\boldsymbol{M}(p,q)$ is symmetric positive semi-definite and rank $\boldsymbol{M}(p,q)$ is 3, which implies that the DAE (II.19.1) is of index 3. For the index 2 formulation, the position constraints are replaced by the velocity constraints

$$0 = \frac{\mathrm{d}}{\mathrm{d}t}\Big(\boldsymbol{g}(p,q) + \boldsymbol{r}(t)\Big) = \boldsymbol{G}(p,q)\begin{pmatrix} \dot{p} \\ \dot{q} \end{pmatrix} + \dot{\boldsymbol{r}}(t). \tag{II.19.2}$$

Additionally, the system is transformed to first order and semi explicit form

$$\begin{aligned} \begin{pmatrix} \dot{p} \\ \dot{q} \end{pmatrix} &= \begin{pmatrix} v_p \\ v_q \end{pmatrix}, \\ \begin{pmatrix} \dot{v}_p \\ \dot{v}_q \end{pmatrix} &= \begin{pmatrix} a_p \\ a_q \end{pmatrix}, \\ 0 &= \boldsymbol{M}(p,q)\begin{pmatrix} a_p \\ a_q \end{pmatrix} - \boldsymbol{f}(p,v_p,q,v_q) + \boldsymbol{G}(p,q)^{\mathrm{T}}\lambda\,, \\ 0 &= \boldsymbol{G}(p,q)\begin{pmatrix} v_p \\ v_q \end{pmatrix} + \dot{\boldsymbol{r}}(t)\,, \end{aligned} \tag{II.19.3}$$

which increases the dimension of the problem to 24. If we define $y := (p,q,v_p,v_q,a_p,a_q,\lambda)^{\mathrm{T}}$, then the consistent values are given by $y(0) := y_0$ and $y'(0) := y_0'$. The components of $y_0$ are zero, except for

| | | | |
|---|---|---|---|
| $y_{0,3}$ | $0.450016933 \cdot 10^{0}$ | $y_{0,16}$ | $-1.344541576709835 \cdot 10^{-3}$ |
| $y_{0,6}$ | $0.103339863 \cdot 10^{-4}$ | $y_{0,17}$ | $-5.062194924490193 \cdot 10^{3}$ |
| $y_{0,7}$ | $0.169327969 \cdot 10^{-4}$ | $y_{0,18}$ | $-6.829725665986310 \cdot 10^{-5}$ |
| $y_{0,8}$ | $0.150000000 \cdot 10^{3}$ | $y_{0,19}$ | $1.813207639590617 \cdot 10^{-20}$ |
| $y_{0,9}$ | $-0.7499576703969453 \cdot 10^{2}$ | $y_{0,20}$ | $-4.268463266810281 \cdot 10^{0}$ |
| $y_{0,10}$ | $-0.2689386719979040 \cdot 10^{-5}$ | $y_{0,21}$ | $2.098339029337557 \cdot 10^{-1}$ |
| $y_{0,11}$ | $0.4448961125815990 \cdot 10^{0}$ | $y_{0,22}$ | $-6.552727150584648 \cdot 10^{-8}$ |
| $y_{0,12}$ | $0.4634339319238670 \cdot 10^{-2}$ | $y_{0,23}$ | $3.824589509350831 \cdot 10^{2}$ |
| $y_{0,13}$ | $-0.1785910760000550 \cdot 10^{-5}$ | $y_{0,24}$ | $-4.635908708561371 \cdot 10^{-9}$ |
| $y_{0,14}$ | $-0.2689386719979040 \cdot 10^{-5}$ | | |

The first 14 components of $y_0'$ read $y_{0,i}' = y_{0,i+7}$, $i = 1, \ldots, 14$; the last 10 are zero.

For the index 2 formulation, the index of the variables $p$, $q$, $v_p$ and $v_q$ equals 1 and that of $a_p$, $a_q$ and $\lambda$ equals 2. The equations are given in detail in the next subsections, in which already some references to the origin of the problem, treated in §19.3, are given.

### 19.2.1 Equations of motion

The position or gross motion coordinates $p$ are

$$p := \begin{pmatrix} \phi_1 \\ \phi_2 \\ x_3 \end{pmatrix} \qquad \begin{matrix} \text{crank angle} \\ \text{connecting rod angle} \\ \text{sliding block displacement} \end{matrix}$$

The deformation coordinates $q$ (of the elastic connecting rod, see below) are

$$q := \begin{pmatrix} q_1 \\ q_2 \\ q_3 \\ q_4 \end{pmatrix} \qquad \begin{matrix} \text{first lateral mode} \sin(\pi x/l_2) \\ \text{second lateral mode} \sin(2\pi x/l_2) \\ \text{longitudinal displacement midpoint} \\ \text{longitudinal displacement endpoint} \end{matrix}$$

The mass matrix $\boldsymbol{M}$ reads

$$\boldsymbol{M}(p,q) = \begin{pmatrix} M_r(p) + M_e(p,q) & C(p,q)^{\mathrm{T}} \\ C(p,q) & M_\Delta \end{pmatrix}$$

with rigid motion mass matrix

$$M_r(p) = \begin{pmatrix} J_1 + m_2 l_1^2 & 1/2\, l_1 l_2 m_2 \cos(\phi_1 - \phi_2) & 0 \\ 1/2\, l_1 l_2 m_2 \cos(\phi_1 - \phi_2) & J_2 & 0 \\ 0 & 0 & m_3 \end{pmatrix},$$

coupling blocks

$$M_e(p,q) = \begin{pmatrix} 0 & \rho l_1 (\cos(\phi_1 - \phi_2) c_1^{\mathrm{T}} + \sin(\phi_1 - \phi_2) c_2^{\mathrm{T}}) q & 0 \\ \rho l_1 (\cos(\phi_1 - \phi_2) c_1^{\mathrm{T}} + \sin(\phi_1 - \phi_2) c_2^{\mathrm{T}}) q & q^{\mathrm{T}} M_\Delta q + 2\rho c_{12}^{\mathrm{T}} q & 0 \\ 0 & 0 & 0 \end{pmatrix}$$

and

$$C(p,q)^{\mathrm{T}} = \begin{pmatrix} \rho l_1 (-\sin(\phi_1 - \phi_2) c_1^{\mathrm{T}} + \cos(\phi_1 - \phi_2) c_2^{\mathrm{T}}) \\ \rho c_{21}^{\mathrm{T}} + \rho q^{\mathrm{T}} B \\ 0^{\mathrm{T}} \end{pmatrix},$$

and elastic body space discretization mass matrix

$$M_\Delta = \rho\, d\, h\, l_2 \begin{pmatrix} 1/2 & 0 & 0 & 0 \\ 0 & 1/2 & 0 & 0 \\ 0 & 0 & 8 & 1 \\ 0 & 0 & 1 & 2 \end{pmatrix}.$$

The forces are given by

$$\boldsymbol{f}(p,\dot{p},q,\dot{q}) = \begin{pmatrix} f_r(p,\dot{p}) + f_e(p,\dot{p},q,\dot{q}) \\ f_\Delta(p,\dot{p},q,\dot{q}) - \text{grad } W_\Delta(q) - D_\Delta \dot{q} \end{pmatrix},$$

where the rigid motion terms are collected in

$$f_r(p,\dot{p}) = \begin{pmatrix} -1/2\, l_1(\gamma(m_1+2m_2)\cos\phi_1 + l_2 m_2 \dot{\phi}_2^2 \sin(\phi_1-\phi_2)) \\ -1/2\, l_2 \gamma m_2 \cos\phi_2 + 1/2\, l_1 l_2 m_2 \dot{\phi}_1^2 \sin(\phi_1-\phi_2) \\ 0 \end{pmatrix}.$$

For the force term $f_e(p,\dot{p},q,\dot{q})$ we have

$$\begin{pmatrix} \rho l_1 \dot{\phi}_2^2(-\sin(\phi_1-\phi_2)c_1^{\mathrm{T}} + \cos(\phi_1-\phi_2)c_2^{\mathrm{T}})q - 2\rho l_1 \dot{\phi}_2(\cos(\phi_1-\phi_2)c_1^{\mathrm{T}} + \sin(\phi_1-\phi_2)c_2^{\mathrm{T}})\dot{q} \\ \rho l_1 \dot{\phi}_1^2(\sin(\phi_1-\phi_2)c_1^{\mathrm{T}} - \cos(\phi_1-\phi_2)c_2^{\mathrm{T}})q - 2\rho\dot{\phi}_2 c_{12}^{\mathrm{T}}\dot{q} - 2\dot{\phi}_2 \dot{q}^{\mathrm{T}} M_\Delta q \\ -\rho\dot{q}^{\mathrm{T}} B \dot{q} - \rho\gamma(\cos\phi_2 c_1^{\mathrm{T}} q - \sin\phi_2 c_2^{\mathrm{T}} q) \\ 0 \end{pmatrix},$$

and for $f_\Delta(p,\dot{p},q,\dot{q})$ the expression

$$\dot{\phi}_2^2 M_\Delta q + \rho\Big(\dot{\phi}_2^2 c_{12} + l_1\dot{\phi}_1^2(\cos(\phi_1-\phi_2)c_1 + \sin(\phi_1-\phi_2)c_2) + 2\dot{\phi}_2 B\dot{q}\Big) - \rho\gamma\Big(\sin\phi_2 c_1 + \cos\phi_2 c_2\Big).$$

The gradient of the elastic potential $W_\Delta(q)$ in case of linear elasticity (which is the default) is grad $W_\Delta(q) = K_\Delta q$ with stiffness matrix

$$K_\Delta = E\, d\, h\, / l_2 \begin{pmatrix} \pi^4/24(h/l_2)^2 & 0 & 0 & 0 \\ 0 & \pi^4 2/3(h/l)^2 & 0 & 0 \\ 0 & 0 & 16/3 & -8/3 \\ 0 & 0 & -8/3 & 7/3 \end{pmatrix}.$$

Alternatively, in case of the nonlinear beam model (`IPAR(1) = 1`, see below), it holds grad $W_\Delta(q) = K_\Delta q + k_\Delta(q)$,

$$k_\Delta(q) = 1/2\,\pi^2\, E\, d\, h / l_2^2 \begin{pmatrix} q_1 q_4 - \beta q_2(-4q_3+2q_4) \\ 4q_2 q_4 - \beta q_1(-4q_3+2q_4) \\ 4\beta q_1 q_2 \\ 1/2 q_1^2 + 2q_2^2 - 2\beta q_1 q_2 \end{pmatrix}, \qquad \beta = 80/(9\pi^2).$$

The damping matrix $D_\Delta$ is by default zero. The coupling matrices and vectors arising from the space discretization read

$$B = d\, h\, l_2 \begin{pmatrix} 0 & 0 & -16/\pi^3 & 8/\pi^3 - 1/\pi \\ 0 & 0 & 0 & 1/(2\pi) \\ 16/\pi^3 & 0 & 0 & 0 \\ 1/\pi - 8/\pi^3 & -1/(2\pi) & 0 & 0 \end{pmatrix}$$

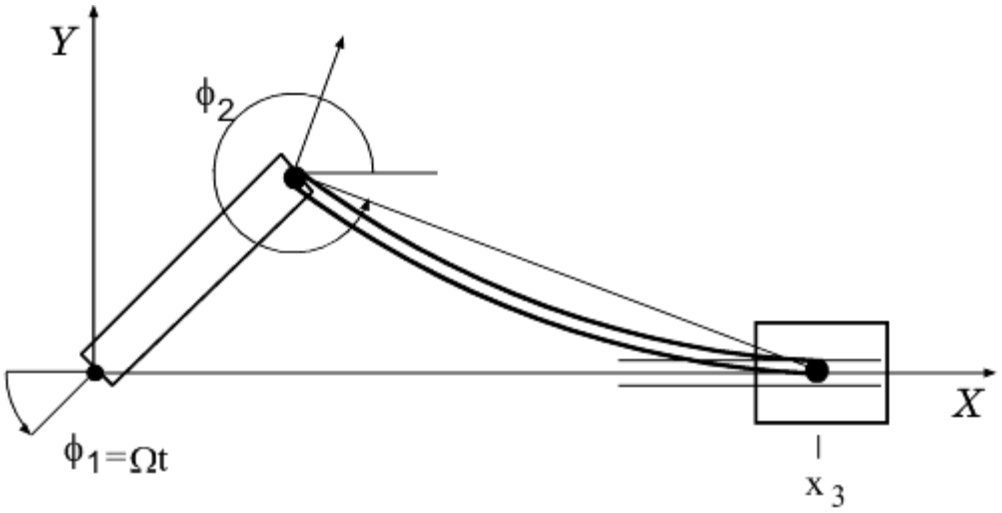


FIGURE II.19.1: The multibody system with crank, connecting rod, sliding block.

and

$$\begin{aligned} c_1 &= d\,h\,l_2(0,\,0,\,2/3,\,1/6)^{\mathrm{T}}, \\ c_2 &= d\,h\,l_2(2/\pi,\,0,\,0,\,0)^{\mathrm{T}}, \\ c_{12} &= d\,h\,l_2^2(0,\,0,\,1/3,\,1/6)^{\mathrm{T}}, \\ c_{21} &= d\,h\,l_2^2(1/\pi,\,-1/(2\pi),\,0,\,0)^{\mathrm{T}}. \end{aligned}$$

Finally, the position constraints $0 = \boldsymbol{g}(p,q) + \boldsymbol{r}(t)$ are given by

$$\begin{aligned} 0 &= l_1 \sin\phi_1 + l_2 \sin\phi_2 + q_4 \sin\phi_2, \\ 0 &= x_3 - l_1 \cos\phi_1 - l_2 \cos\phi_2 - q_4 \cos\phi_2, \\ 0 &= \phi_1 - \Omega t\,. \end{aligned}$$

### 19.2.2 Parameters

For the simulation, the following data are used:
The bodies have lengths $l_1 = 0.15$, $l_2 = 0.30[m]$.
The masses of the bodies are $m_1 = 0.36$, $m_2 = 0.151104$, $m_3 = 0.075552[kg]$.
The moments of inertia are $J_1 = 0.002727$, $J_2 = 0.0045339259[kg\,m^2]$.
The flexible connecting rod has height and width $h = d = 0.008[m]$.
The mass density $\rho = 7870[kg/m^3]$, and Young's modulus $E = 2.\cdot 10^{11}[N/m^2]$.
The gravity constant was set to zero since gravitation plays no role here, $\gamma = 0$.
The angular velocity of the prescribed crank motion is $\Omega = 150[rad/s]$.

## 19.3 Origin of the problem

The planar slider crank mechanism, see Figure II.19.1, consists of a rigid crank (body 1), an elastic connecting rod (body 2), a rigid sliding block (body 3) and two revolving and one translational joint. Koppens [Kop89] and Jahnke [JPD93] investigated this example using an ODE model in minimum coordinates. In [Sim96], an alternative DAE approach is introduced.

The mathematical model outlined above is derived in two steps. First, the elastic connecting rod is discretized in space. The geometry of the rod allows to apply an Euler-Bernoulli beam

$$\begin{aligned} u_1(x,y) &= w_1(x) - y w_2'(x), \\ u_2(x,y) &= w_2(x), \end{aligned}$$

to describe the longitudinal and lateral displacements $u_1$ and $u_2$ of material point $(x, y)$ in the body-fixed coordinate system. For the longitudinal displacement $w_1$ of the neutral fiber, a simple quadratic model

$$w_1(x) \doteq \xi^2(-4q_3 + 2q_4) + \xi(4q_3 - q_4), \qquad \xi = x/l_2,$$

is sufficient to show the basic effects. The lateral displacement $w_2$ is approximated by the first two sinus shape functions

$$w_2(x) \doteq \sin(\pi\xi)q_1 + \sin(2\pi\xi)q_2\,.$$

These functions satisfy the boundary conditions $w_1(0) = 0$, $w_2(0) = 0$, $w_2(l_2) = 0$. Accordingly, the body-fixed coordinate system's origin is placed in $(x, y) = (0, 0)$, and its $x$-axis passes through the point $(l_2 + w_1(x), 0)$.

As already mentioned in §19.2, we provide two versions of the problem. The first one (default) assumes linear elasticity while the second takes the coupling of longitudinal and lateral displacements in terms of $k_\Delta(q)$ into account. Set `IPAR(1) = 1` to switch to this nonlinear beam model. See below for a comparison of the results.

In the second step, the equations of motion of the overall multibody system are assembled. Due to the choice of $\phi_2$ as gross motion coordinate, there is no constraint equation necessary to express the revolving joint between crank and connecting rod. The revolving joint between sliding block and connecting rod and the translational joint lead to two constraints that depend on the deformation variable $q_4$. The third constraint equation defines the crank motion using $\boldsymbol{r}(t) = (0,\, 0,\, -\Omega t)^{\mathrm{T}}$. Here, other functions for the crank motion could also be prescribed.

The model described so far features no dissipation. Consequently, the solutions show a purely oscillatory behavior. We supply also a nonzero damping matrix $D_\Delta$ which can be activated by setting `IPAR(2) = 1`. Then, 0.5 percent dissipation is included in the right hand side of the elastic connecting rod.

In §19.4, we investigate the dynamic behavior of the slider crank model corresponding to the nonlinear model without damping with the initial values listed in §19.2, which were calculated such that the motion is almost smooth, using an asymptotic expansion technique [Sim97]. In Figure II.19.4 we see the behavior of the numerical solution for this setting of the model. A close look at these plots reveals that both lateral displacements $q_1, q_2$ as well as longitudinal displacements $q_3, q_4$ still show some small oscillations. The corresponding frequencies as solutions of the eigenvalue problem $\omega^2 M_\Delta q = K_\Delta q$ are

$$\omega_1 = 1277, \quad \omega_2 = 5107, \quad \omega_3 = 6841, \quad \omega_4 = 24613 \;\; [rad/s]\,.$$

In particular, $q_3$ and $q_4$ are characterized by the relatively large frequency $\omega_4$. Any explicit discretization in time will need stepsizes smaller than the shortest period of oscillation, even for tracking a smooth solution. On the other hand, the challenge for implicit methods is to be able to take larger steps. In this simulation the gross motion coordinates $p$ differ only slightly from the motion of a mechanism with rigid connecting rod.

The subroutines that describe the model offer several possibilities to test other variants of the model than those tested in §19.4. We now discuss some of them.

### Oscillatory solution

We provide also a second set of initial values (`subroutine init2`) which lead to a strongly oscillatory solution. Here, the initial deformation as well as the corresponding velocity were set to zero, $q(0) =$

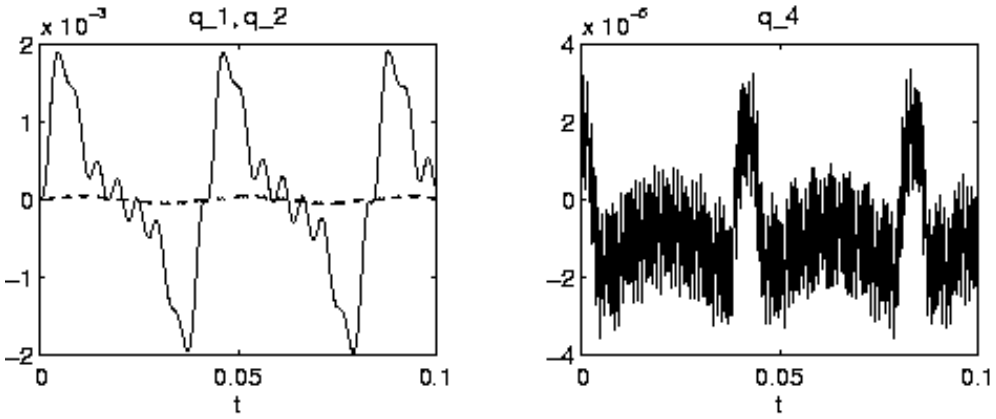


FIGURE II.19.2: Solution of slider crank for 'rigid' initial values, i.e., deformation $q(0) = v_q(0) = 0$.

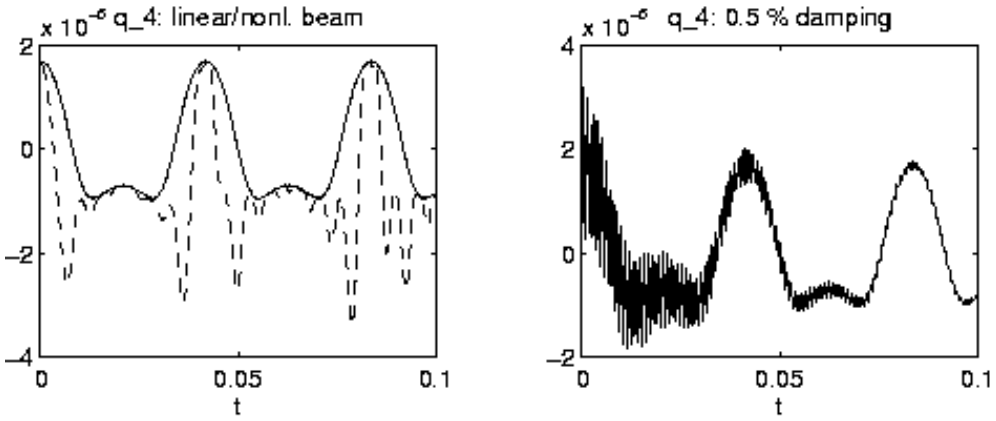


FIGURE II.19.3: Left: Comparison of linear and nonlinear beam model. Right: Oscillatory solution with physical damping.

$v_q(0) = 0$, which is equivalent to consistent initial values on a rigid motion trajectory. Figure II.19.2 plots the behavior of $q_1$, $q_2$ and $q_4$ for this setting. Both lateral and longitudinal modes oscillate now with different frequencies.

### Nonlinear beam model and damping

The left and right plot in Figure II.19.3 show the effects of setting `IPAR(1) = 1` and `IPAR(2) = 1`, respectively. On the left, the difference between linear and nonlinear beam model is illustrated, with initial values close to the smooth motion. In particular, the components $q_3$ and $q_4$ change if the nonlinear model is employed. At points of maximum bending, the longitudinal displacement has now much smaller minima. If we increase the crank's angular velocity, the resulting forces acting on the connecting rod are much larger and we can then even observe how the sharp needles turn into a singularity, the buckling phenomenon.

On the right of Figure II.19.3, the damping was activated by `IPAR(2) = 1`, with initial values on a rigid motion trajectory (`init2`). Obviously, the oscillation shown in Figure II.19.2 on the right is now slowly damped out.

TABLE II.19.1: *Failed runs.*

| solver | $m$ | reason |
|---|---|---|
| MEBDFDAE | $19, \ldots, 24$ | stepsize too small |
| MEBDFI | $21, 22, 23, 24$ | stepsize too small |
| PSIDE-1 | $17, 18, \ldots, 24$ | iteration matrix singular |
| RADAU | 24 | core dump / overflow in decomposition |
| RADAU5 | 24 | core dump / overflow in decomposition |

TABLE II.19.2: *Reference solution at the end of the integration interval.*

| | | | |
|---|---|---|---|
| $y_1$ | $1.500000000000104 \cdot 10^{1}$ | $y_{13}$ | $4.974111734266989 \cdot 10^{-4}$ |
| $y_2$ | $-3.311734988256260 \cdot 10^{-1}$ | $y_{14}$ | $1.105560003626645 \cdot 10^{-3}$ |
| $y_3$ | $1.697373328427860 \cdot 10^{-1}$ | $y_{15}$ | $0$ |
| $y_4$ | $1.893192899613509 \cdot 10^{-4}$ | $y_{16}$ | $6.488737541276957 \cdot 10^{3}$ |
| $y_5$ | $2.375751249879174 \cdot 10^{-5}$ | $y_{17}$ | $2.167938629509884 \cdot 10^{3}$ |
| $y_6$ | $-5.323896770569702 \cdot 10^{-6}$ | $y_{18}$ | $3.391137060286523 \cdot 10^{1}$ |
| $y_7$ | $-8.363313279112129 \cdot 10^{-6}$ | $y_{19}$ | $1.715134772216488 \cdot 10^{-1}$ |
| $y_8$ | $1.500000000000000 \cdot 10^{2}$ | $y_{20}$ | $-1.422449408912512 \cdot 10^{0}$ |
| $y_9$ | $6.025346755138369 \cdot 10^{1}$ | $y_{21}$ | $1.003946428124810 \cdot 10^{0}$ |
| $y_{10}$ | $-8.753116326670527 \cdot 10^{0}$ | $y_{22}$ | $-6.232935833287916 \cdot 10^{1}$ |
| $y_{11}$ | $-3.005541400289738 \cdot 10^{-2}$ | $y_{23}$ | $-1.637920993367306 \cdot 10^{2}$ |
| $y_{12}$ | $-5.500431812571696 \cdot 10^{-3}$ | $y_{24}$ | $2.529857947066878 \cdot 10^{1}$ |

## 19.4 Numerical solution of the problem

The results presented here refer to index 2 formulation of the linear model without damping, using the initial values corresponding to a smooth solution.

Tables II.19.2–II.19.3 and Figures II.19.4–II.19.8 present the reference solution at the end of the integration interval, the run characteristics, the behavior of some of the solution components over the integration interval and the work-precision diagrams, respectively. In computing the scd values, only the first seven and the last three components were taken into account, since they refer to the physically important quantities. The reference solution was computed using MEBDFI with atol $= 10^{-14}$ and rtol $= 10^{-14}$ and h0 $= 10^{-12}$. For the work-precision diagrams, we used: rtol $= 10^{-(4+m/4)}$, $m = 0, \ldots, 24$; atol = rtol; h0 $= 10^{-2} \cdot$ rtol for BIMD, GAMD, MEBDFDAE, MEBDFI, RADAU5 and RADAU. The failed runs are in Table II.19.1; listed are the name of the solver that failed, for which values of $m$ this happened, and the reason for failing.

.

### Remarks

- The slider crank is an example for a stiff mechanical system given in DAE form. See Lubich [Lub93] for an investigation of such systems and the implications for numerical methods in the ODE case.
- The nonlinear beam model leads to a higher computational effort but does not provoke convergence failures of Newton's method in RADAU5, as might be expected in case of nonlinear stiffness terms.

TABLE II.19.3: *Run characteristics.*

| solver | rtol | atol | h0 | mescd | scd | steps | accept | #f | #Jac | #LU | CPU |
|---|---|---|---|---|---|---|---|---|---|---|---|
| BIMD | $10^{-4}$ | $10^{-4}$ | $10^{-6}$ | 0.23 | 2.50 | 102 | 102 | 1762 | 102 | 102 | 0.0420 |
| | $10^{-6}$ | $10^{-6}$ | $10^{-8}$ | 0.39 | 3.38 | 1155 | 1155 | 22548 | 1155 | 1155 | 0.5144 |
| | $10^{-8}$ | $10^{-8}$ | $10^{-10}$ | 2.50 | 5.49 | 992 | 992 | 35662 | 992 | 992 | 0.7086 |
| GAMD | $10^{-4}$ | $10^{-4}$ | $10^{-6}$ | 0.23 | 2.28 | 60 | 60 | 1983 | 60 | 60 | 0.0342 |
| | $10^{-6}$ | $10^{-6}$ | $10^{-8}$ | −0.16 | 2.83 | 534 | 527 | 25206 | 527 | 534 | 0.4089 |
| | $10^{-8}$ | $10^{-8}$ | $10^{-10}$ | 1.70 | 4.69 | 650 | 650 | 46109 | 650 | 650 | 0.7271 |
| MEBDFI | $10^{-4}$ | $10^{-4}$ | $10^{-6}$ | 0.22 | 1.49 | 250 | 242 | 1593 | 28 | 28 | 0.0176 |
| | $10^{-6}$ | $10^{-6}$ | $10^{-8}$ | 0.03 | 3.03 | 3328 | 3324 | 15099 | 170 | 170 | 0.2011 |
| | $10^{-8}$ | $10^{-8}$ | $10^{-10}$ | 2.72 | 5.71 | 6316 | 6315 | 28395 | 313 | 313 | 0.3845 |
| PSIDE-1 | $10^{-4}$ | $10^{-4}$ | | −0.05 | 0.93 | 45 | 41 | 858 | 29 | 180 | 0.0234 |
| | $10^{-6}$ | $10^{-6}$ | | 0.16 | 2.43 | 259 | 235 | 5020 | 147 | 888 | 0.1298 |
| | $10^{-8}$ | $10^{-8}$ | | 1.66 | 4.66 | 1639 | 1445 | 31526 | 54 | 2324 | 0.6412 |
| RADAU | $10^{-4}$ | $10^{-4}$ | $10^{-6}$ | 0.20 | 1.90 | 104 | 92 | 717 | 89 | 104 | 0.0224 |
| | $10^{-6}$ | $10^{-6}$ | $10^{-8}$ | 0.14 | 2.89 | 132 | 131 | 3367 | 123 | 131 | 0.0654 |
| | $10^{-8}$ | $10^{-8}$ | $10^{-10}$ | 1.65 | 4.65 | 420 | 419 | 10589 | 397 | 414 | 0.2089 |

- As an alternative to stiff solvers, it is still possible to apply methods based on explicit discretizations, e.g., half-explicit or projection methods for constrained mechanical systems. The code MDOP5 [Sim95], a projection method based on DOPRI5, uses 2260 integration steps to solve this problem in the default setting, with atol = $10^{-6}$ and rtol = $10^{-5}$, and initial values close to the smooth motion. Thus, the stiffness is no that severe in case of this carefully chosen one-dimensional elastic body model.
- There is also an extended version of the slider crank with a two-dimensional FE grid for the connecting rod. There, explicit methods do not work any longer. An animation of the system motion can be found at `http://www.mathematik.tu-darmstadt.de/~ simeon/` .

## References

[JPD93] M. Jahnke, K. Popp, and B. Dirr. Approximate analysis of flexible parts in multibody systems using the finite element method. In Schiehlen W., editor, *Advanced Multibody System Dynamics*, pages 237–256, Stuttgart, 1993. Kluwer Academic Publishers.

[Kop89] W. Koppens. *The dynamics of systems of deformable bodies.* PhD thesis, Technische Universiteit Eindhoven, 1989.

[Lub93] C. Lubich. Integration of stiff mechanical systems by Runge-Kutta methods. *ZAMP*, 44:1022–1053, 1993.

[MM08] F. Mazzia and C. Magherini. *Test Set for Initial Value Problem Solvers, release 2.4.* Department of Mathematics, University of Bari and INdAM, Research Unit of Bari, February 2008. Available at `http://www.dm.uniba.it/~testset`.

[Sim95] B. Simeon. MBSPACK - Numerical integration software for constrained mechanical motion. *Surv. on Math. in Ind.*, 5:169–202, 1995.

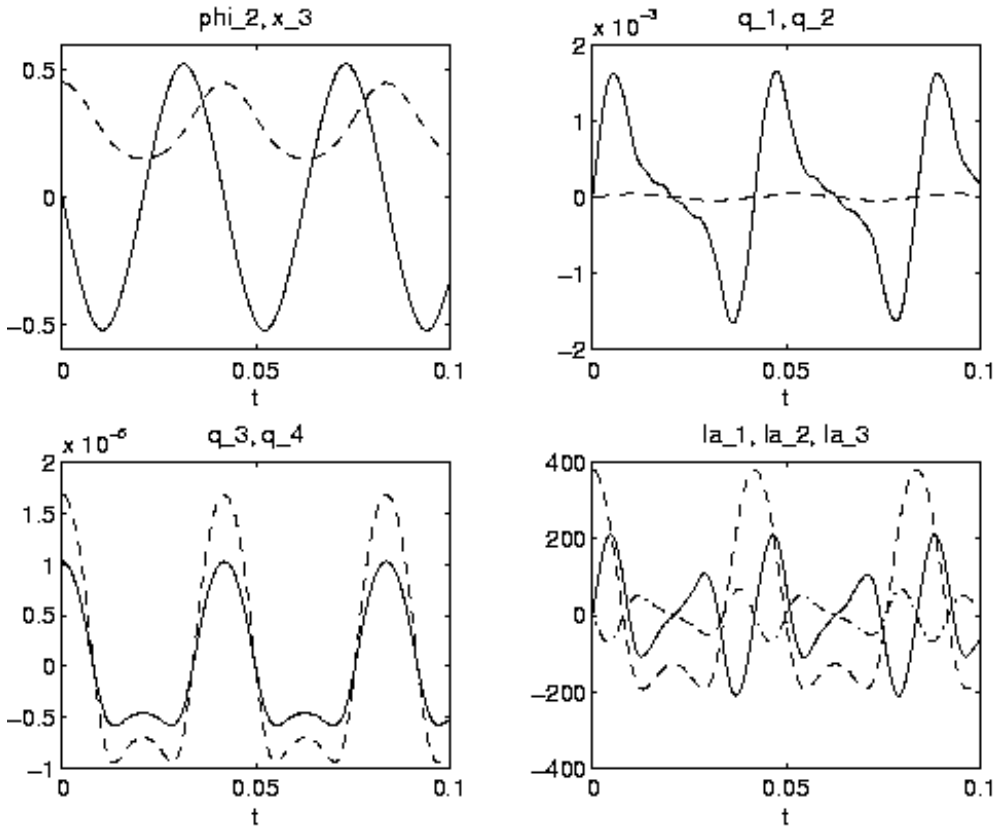


FIGURE II.19.4: *Behavior of the ith solution component;* $i \in \{2, 3, \ldots, 7, 22, 23, 24\}$.

[Sim96] B. Simeon. Modelling a flexible slider crank mechanism by a mixed system of DAEs and PDEs. *Math. Modelling of Systems*, 2:1–18, 1996.

[Sim97] B. Simeon. DAEs and PDEs in elastic multibody systems, 1997. *To appear in Numerical Algorithms.*

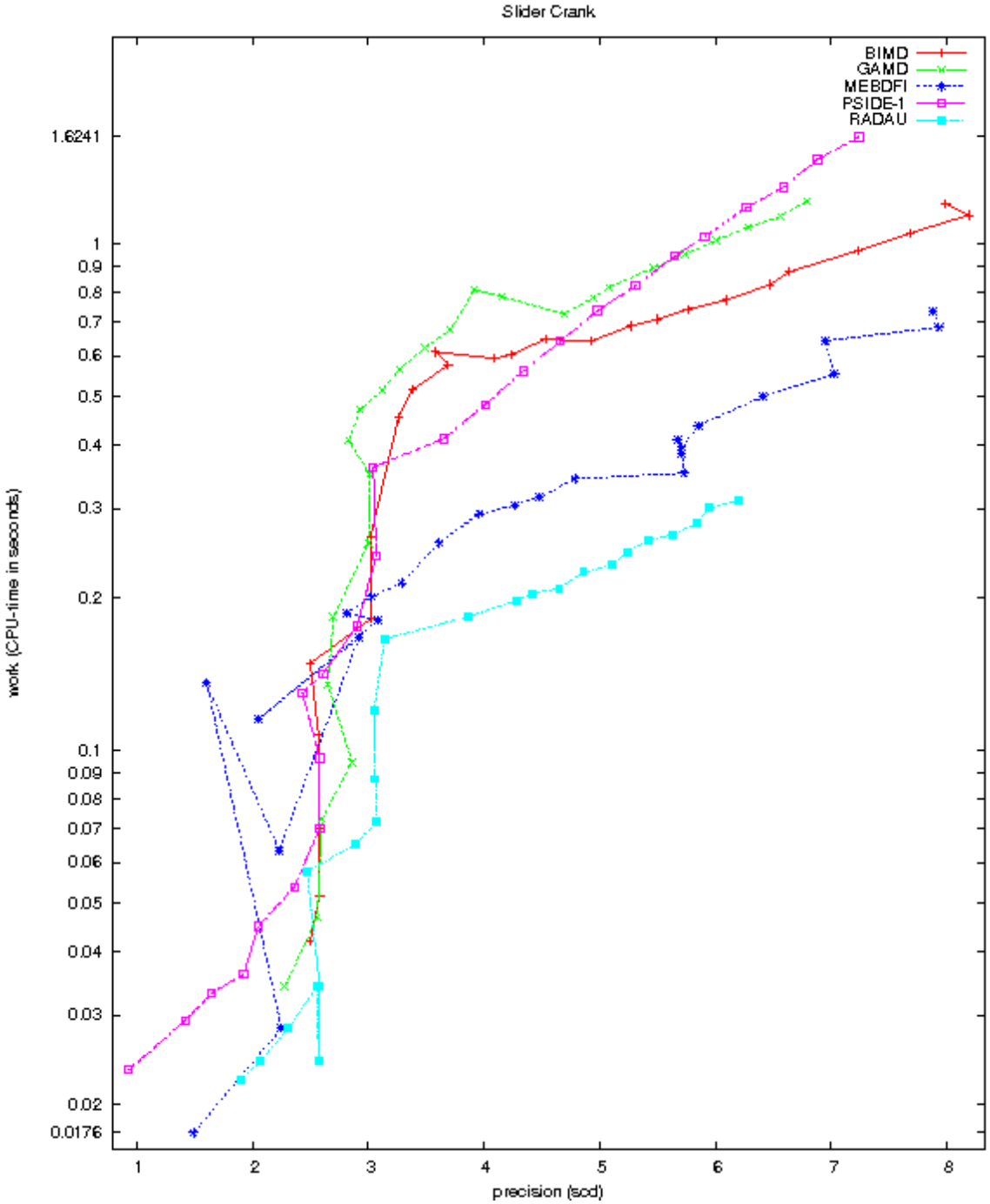


FIGURE II.19.5: *Work-precision diagram (scd versus CPU-time).*

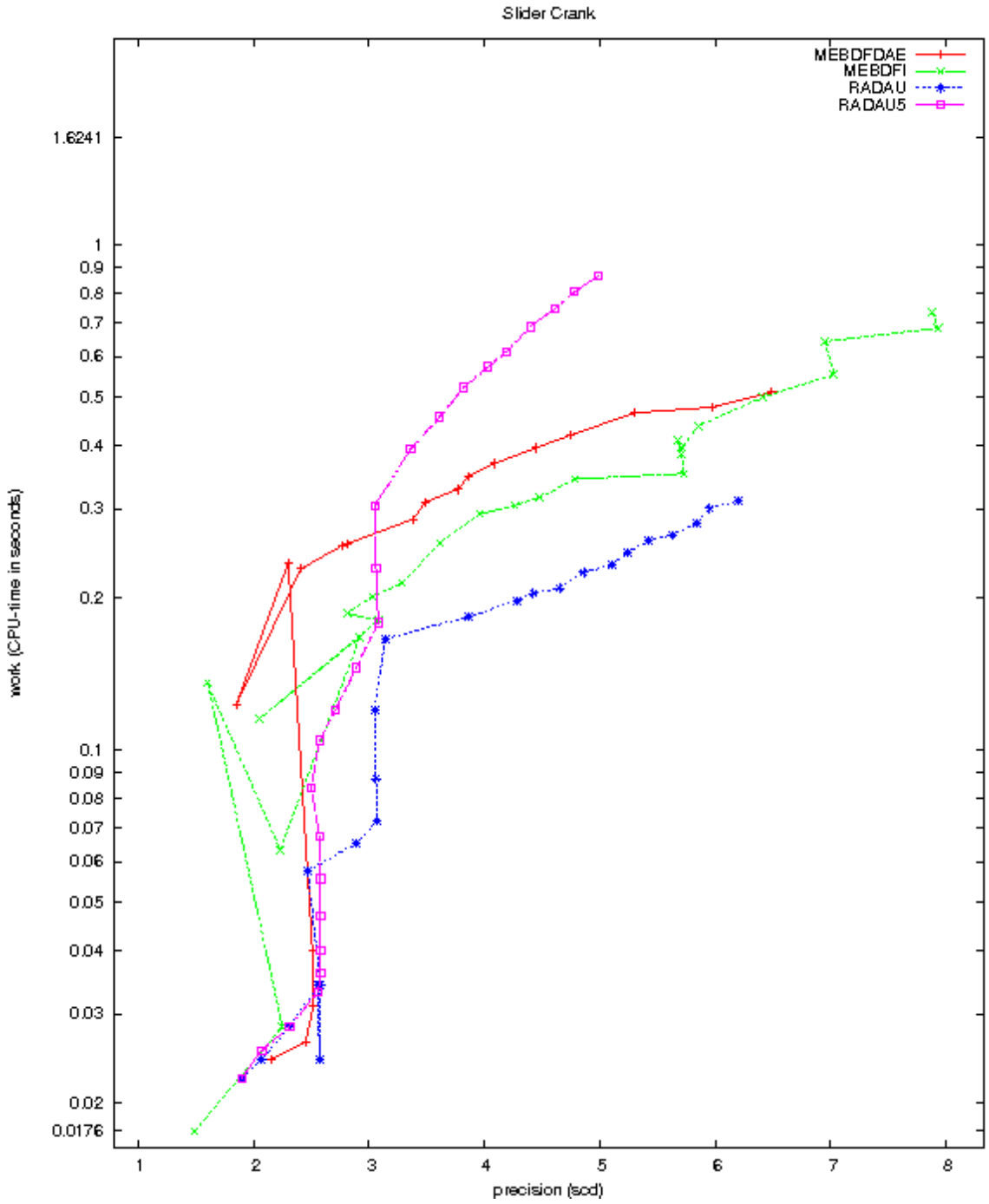


FIGURE II.19.6: *Work-precision diagram (scd versus CPU-time).*

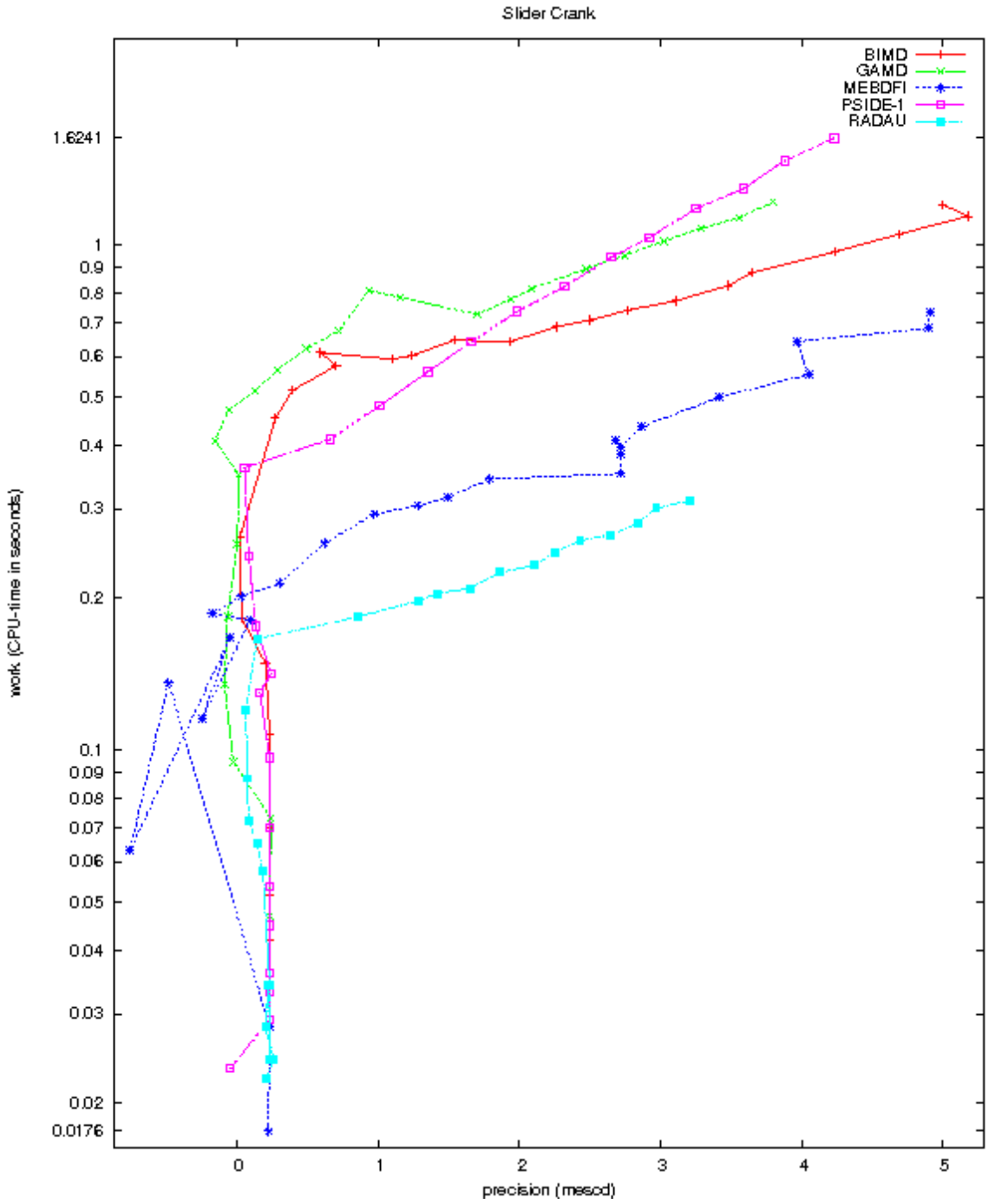


FIGURE II.19.7: *Work-precision diagram (mescd versus CPU-time).*

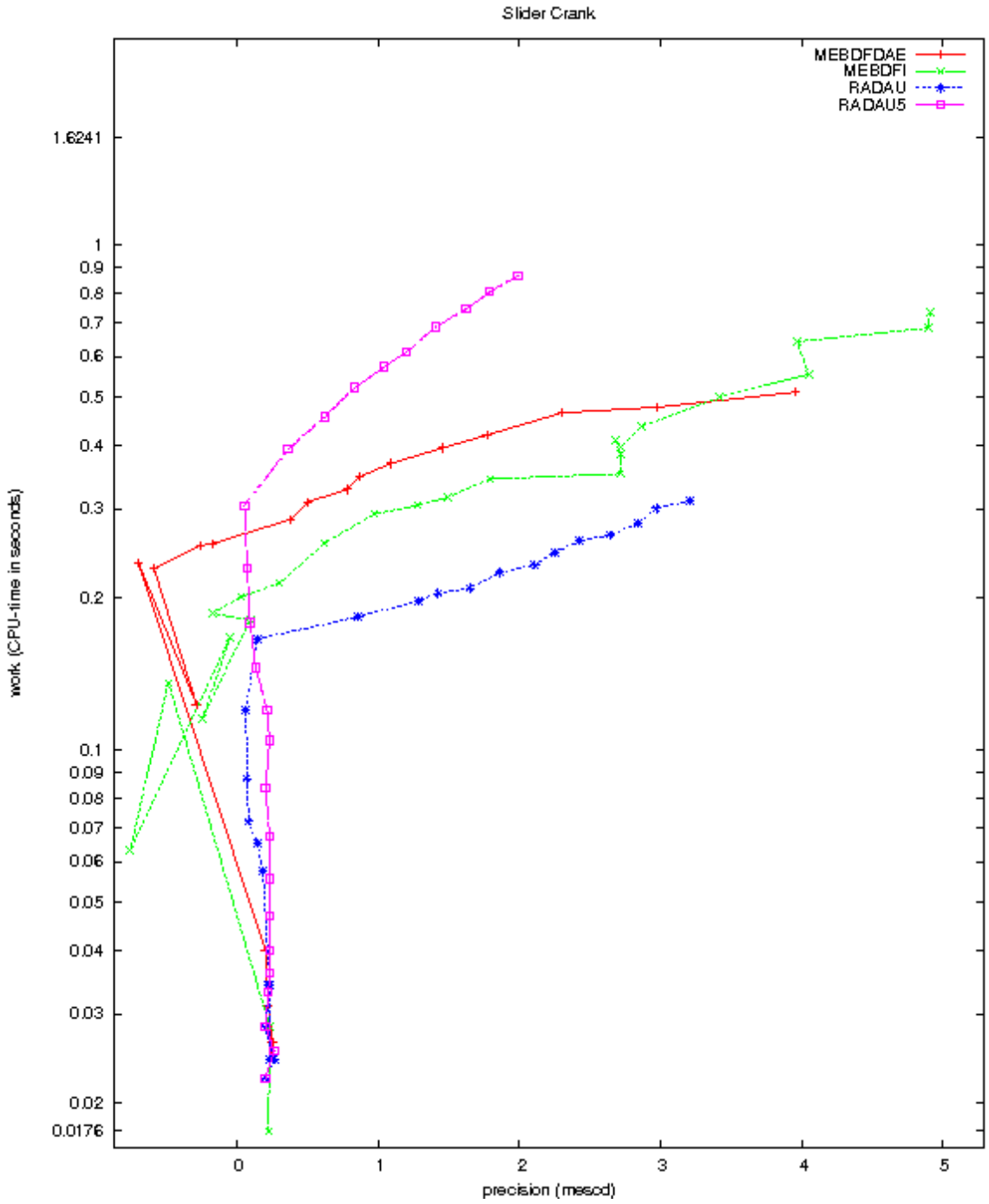


FIGURE II.19.8: *Work-precision diagram (mescd versus CPU-time).*